Early View publication on
www.wileyonlinelibrary.com
(issue and page numbers not yet assigned;
citable using Digital Object Identifier – **DOI**)

J. Biophotonics 1–11 (2012) / **DOI** 10.1002/jbio.201200094

Journal of
BIOPHOTONICS

FULL ARTICLE

Detection of recombinant growth hormone by evanescent cascaded waveguide coupler on silica-on-silicon

*Jayan Ozhikandathil and Muthukumaran Packirisamy**

Optical Bio-Microsystems Laboratory, Dept. of Mechanical and Industrial Engineering, Concordia University, Montreal, Canada, H3G 1M8

Received 22 May 2012, revised 21 June 2012, accepted 8 July 2012
Published online 26 July 2012

Key words: Evanescent wave sensor, silica-on-silicon, growth hormone, FDTD

An evanescent wave based biosensor is developed on the silica-on-silicon (SOS) with a cascaded waveguide coupler for the detection of recombinant growth hormone. So far, *U*-bends and tapered waveguides are demonstrated for increasing the penetration depth and enhancing sensitivity of the evanescent wave sensor. In this work, a monolithically integrated sensor platform containing a cascaded waveguide coupler with optical power splitters and combiners designed with *S*-bends and tapper waveguides is demonstrated for an enhanced detection of recombinant growth hormone. In the cascaded waveguide coupler, a large surface area to bind the antibody with increased penetration depth of evanescent wave to excite the tagged-rbST is obtained by splitting the waveguide into multiple paths using *Y* splitters designed with *s*-bends and subsequently combining them back to a single waveguide through tapered waveguide and combiners. Hence a highly sensitive fluoroimmunoassay sensor is realized. Using the 2D FDTD (Finite-difference time-domain method) simulation of waveguide with a point source in Rsoft FullWAVE, the fluorescence coupling efficiency of straight and bend section of waveguide is analyzed. The sensor is demonstrated for the detection of fluorescently-tagged recombinant growth hormone with the detection limit as low as 25 ng/ml.

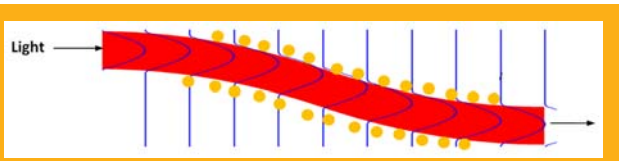

Evanescent wave sensor

1. Introduction

The bovine growth hormone, also called bovine somatotropin (bST) is a naturally produced peptide hormone in cow, which has strong influences on the biological effects such as growth, developments and reproductive functions. The effect of bST on the production of milk was identified in 1937 [1]. Since then, bST has been used for increasing the production of milk and meat. Since 80's, with the emergence of the recombinant DNA technology, large quantities of artificial hormones called recombinant bovine growth hormone also known as recombinant bovine somatotropin (rbST), are produced and extensively used for the production of milk and meat. Use of growth hormones for the production of milk and meat is still controversial [2–4] due to its potential effects on animal and human health. Hence, there is a huge demand for a highly sensitive, rapid and a low cost method for the detection of growth hormones in dairy industries.

* Corresponding author: e-mail: pmuthu@alcor.concordia.ca

The existing methods of detecting peptides include the enzyme-linked immunosorbent assay (ELISA) [5, 6], radioimmunoassay (RIA) [7, 8], bioassay methods [9], etc. Although the ELISA is a widely used method of detection of protein due to simplicity and low cost, it is a time consuming process, and it detects the antibody in a relative term such as "titer" that is a combination of affinity and concentration. Recently, the liquid chromatography-mass spectrometry (LC-MS) combined with electrospray ionization [10–12] has been demonstrated as a powerful techniques for the detection of rbST, which could discriminate the recombinant and endogenous forms of the somatotropin. However, the LC-MS is a complex technique and requires expensive instrumentations. A surface plasmon based biosensor [13] is reported for the injection preparations by using the expensive instrumentation. In this work, a novel evanescent wave sensor, fabricated on the silica-on-silicon waveguide is proposed for the detection of fluorophore tagged recombinant bovine growth hormone.

Among the various methods of bio-detection, optical-methods by using fluorescence [14], surface plasmon resonance (SPR) [15] and evanescent wave-based methods [16, 17] are attractive approaches due to their higher sensitivity, better stability, better spatial resolution and high discrimination capability. Evanescent wave sensing methods have been widely reported for chemical and biological detection [18, 19]. The evanescent wave is the exponentially decaying tail of the guided mode in an optical waveguide, which is highly suitable for the transduction of surface-assisted phenomena that occur in the close proximity of the surface of the core of the waveguide. Evanescent wave based detection can be employed in both absorption and fluorescence modes. For the evanescence absorption sensors, the biomolecules are immobilized on the core of the waveguide, hence, the loss of the propagating waves due to the absorption of evanescent wave is used as the sensing mechanism. The absorption based detection is one of the earliest bio-detection methods, which is limited to the biomolecules having the chromophores which are responsible for the absorption of light. In the fluorescence sensor, the biomolecules are conjugated with certain fluorescent dyes and detected by exciting the conjugates and measuring the fluorescence emission. The conjugates can be selectively adsorbed onto the waveguide surfaces having the immobilized antibody, thereby exciting the conjugates which are closely bound to the core of the waveguide by the evanescent wave. The fluorescence signal emitted by the conjugates is coupled back to the waveguide and analyzed by spectroscopy.

Evanescent wave sensors are implemented by using optical fibers [20] or planar waveguides [21]. In optical fiber-based evanescent wave sensor, the thickness of the cladding is reduced or removed so that the evanescent wave can interact with the species immobilized on the fiber. When the cladding is completely removed, the uncladed section of the fiber can be dipped directly in the aqueous buffer solution containing species for the sensing experiments. However, the mismatch in the *V*-number between the uncladded and cladded section of the fiber reduces the fluorescence collection efficiency for the fluorescence based evanescent sensors. V-number is an approximate number of propagating modes in the waveguides. The sensitivity of the evanescent wave sensors implemented by a straight waveguide with uniform diameter is less as the depth of penetration of evanescent wave is limited for such a configuration. Hence the length of the species evanescent-wave interaction length needs to be increased to achieve higher sensitivity. The evanescent penetration depth in a waveguide is given by:

$$d_p = \frac{\lambda}{2 \times \pi \times n_c(\sin^2 \theta - \sin^2 \theta_c)} \quad (1)$$

Where λ is the free space wavelength of the light propagating through the waveguide, n_c is the refractive index of core, θ is the angle of ray at the core-cladding interface with respect to the normal and θ_c is the critical angle. It can be seen from Eq. (1) that the d_p is maximum when θ approaches the critical angle. Therefore, alternative methods reported to increase the evanescent wave penetration depth are selective ray launching [22], use of fiber probes with tapered geometry [23] and use of bends [24] in waveguides. The tapering of the fiber probe could increase the evanescent wave penetration depth and also reduces the mismatch in *V*-numbers. The bending of the fiber could bring the angle θ close to the critical angle, which transfers power from the guided modes to the leaky modes and hence more light is available to excite the tagged-species. The unclad fiber probes with U-bend is reported [24, 25] for enhancing the detection of bio-species. The U-bend could extend the evanescent wave deeper into the surrounding medium and hence the sensitivity has been increased.

Although the optical fibers are more versatile and easily available, planar waveguide sensors have several advantages. The mechanical robustness, feasibility of integration of multiple optical and microfluidics components for the realization of lab-on-a-chips, and the easiness of immobilizing biospecies for the specific detection are the major advantages of the planar waveguides over optical fiber based sensors. In this work, silica-on-silicon (SOS) waveguide is used for the realization of an evanescent wave sensor. SOS has been proven to be a low-cost and good platform for the integrated optical circuits as the existing well-characterized semiconductor pro-

cessing techniques can be readily adopted for the fabrication of high quality oxide films necessary for the fabrication of low loss optical waveguides. SOS is also suitable for the integration of microfluidic components [26], hence the realization of miniaturized analytical systems is possible. In this work, a cascaded waveguide coupler system, monolithically integrated on SOS platform was used for the detection of the recombinant bovine growth hormone. The waveguide pattern composed of a single waveguide split into multiple paths using *s*-bend couplers and subsequently combined to single waveguide was monolithically integrated on the SOS platform. The fluorescently tagged-rbST molecules are immobilized on the surface of the waveguide. By splitting of the waveguide into multiple paths, more area is available to immobilize the tagged-rbST. In addition, the penetration depth of the evanescent wave can be increased with the use of the *s*-bend and taper. In this paper, an evanescent wave sensor with enhanced sensitivity is realized by using cascaded waveguide coupler integrated with *s*-bends, tapers and splitters. A novel cascaded waveguide coupler (CWC) is proposed for the realization of an evanescent wave sensor and sensitivity of the CWC is compared with single waveguide.

2. Evanescent wave fluorescence sensor

A schematic illustration of the evanescent wave fluorescence sensor is shown in Figure 1. A *s*-bend section with fluorescently tagged bio-species placed around the core of the waveguide is shown in Figure 1(a). As the light propagate through the waveguide, the evanescent tail of the propagating wave

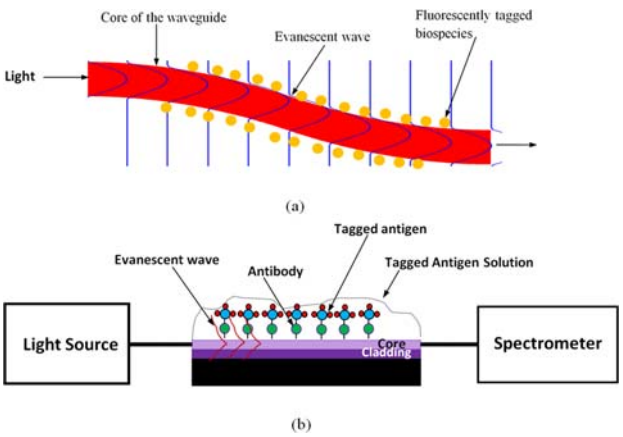

Figure 1 (online color at: www.biophotonics-journal.org) (**a**) Evanescent wave sensor, (**b**) Sketch of the SOS waveguide with antibody and tagged-antigen immobilized on core.

can excite the tagged bio-species and the emitted fluorescence signals are coupled back to waveguide and analyzed.

In the SOS waveguide, two silicon dioxide layers of different refractive indices (RI) are deposited on the silicon wafer. The first layer with lower refractive index acts as a bottom cladding layer and the second layer with higher refractive index acts as a core of the waveguide. The antibody corresponding to the rbST is adsorbed on the core for the selective binding of the fluorescently tagged-rbST. The buffer solution containing the tagged-rbST is placed on the core, hence the solution containing bio-species acts as a top cladding layer of the waveguide (Figure 1(b)). The antibody immobilized on the core interacts and binds with tagged-rbST on evanescent field of the core. Therefore, the tagged-rbST available within the vicinity of evanescent field are excited. The fluorescence signal emitted by the tagged-rbST is coupled back to the core through multiple waveguides of the coupler and propagated through the waveguide and coupled to the spectrometer. The mechanism of the back-coupling of the fluorescence is explained in Ref. [27]. The back-coupled fluorescence occurs when the oscillations of the excited dipoles of the flurophores which are closely bound to the core produce the electromagnetic near field and overlap with the evanescent tail of the guided modes and meet the conditions for the propagation of light in the waveguide. The theoretical and experimental investigation reported on the fluorescence collection efficiency of the fiber [28] and planar waveguide [21] structures demonstrate that the fluorescence collection efficiency increases with the *V*-number of the waveguide.

In this work, the fluorescence collection efficiency of the straight and *s*-bend are simulated by FDTD techniques. The *s*-bend is chosen as it can be a basic element of the proposed cascaded waveguide coupler for enhancing the detection efficiency.

3. Estimation of fluorescence collection efficiency of straight and *s*-bend waveguides

As explained before, in the evanescent-wave fluorescence sensors, the fluorophore-tagged biomolecules are selectively adsorbed to the core by the functionalized antibody molecules. The fluorescently-tagged molecules are excited by the evanescent tail of the propagating wave and the fluorescence signals emitted by the fluorophores are collected back to the core.

Ray optics is insufficient to explain the coupling of light from a light source located at the cladding of the waveguide. Using the Snell's law, it can be seen that any light beam that can penetrate into the core

from the cladding cannot satisfy the condition for total internal reflection, hence the rays that are refracted into the core leak out rapidly after few reflections at the core-cladding interface. However, by using the wave optics, we can see that the light sources located near the core-cladding interface can interact with evanescent tail of the guided modes by transferring some of the power from the light source to the guided mode by the evanescent wave coupling.

In order to estimate fluorescence collection efficiency of the straight and bend waveguides, FDTD simulation by using RSoft FullWAVE was carried out. A 2D model of waveguide with a point source of wavelength of 650 nm placed in the cladding near to the core was used for the FDTD simulation. A power monitor was placed at the end of the waveguide. The "fluorescence collection efficiency" is defined as the ratio of total power received in a power monitor to the total power radiated by the point source. The total power emitted by the point source is set to unity.

3.1 The fluorescence collection efficiency of straight waveguide

Figure 2(a) and (b) show the waveguide with a point source modeled in the FDTD and the refractive index distribution of the model, respectively. In the sensor configuration, tagged-rbST suspended in PBS solution having the refractive index of 1.33 is dropped directly on the waveguide with a core made up of silica having the refractive index of 1.46. Therefore the refractive indices of the core and cladding are set to 1.46 and 1.33 respectively for silica and biological solution for the simulation. The length, L of waveguide is kept at 100 μm and the width, W was varied from the 5 μm to 20 μm. The dependence of the location of light source on the collection efficiency was investigated fist, and then the simulation was carried out by changing the width of the waveguide W. The distance d of the light source from the core was varied from 50 nm to 1000 nm.

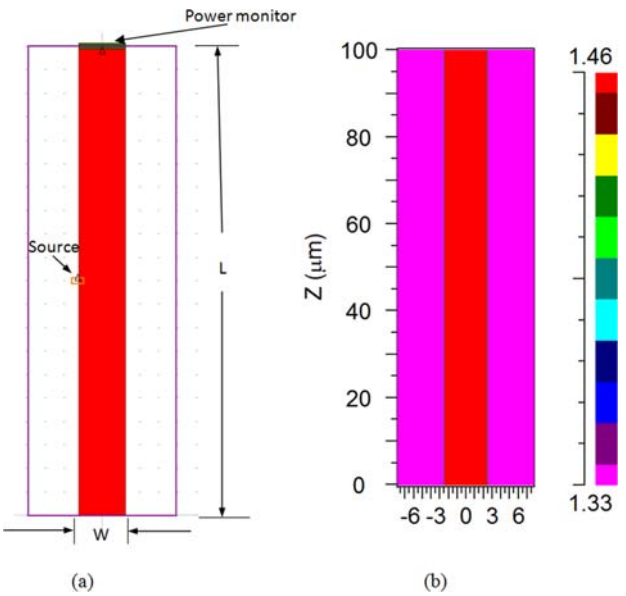

Figure 2 (online color at: www.biophotonics-journal.org) (**a**) The FDTD model of waveguide with a point source (**b**) refractive index distribution of the model.

Figure 3(a) shows the FDTD simulation showing the coupling of light from a point source kept at the cladding to the propagation mode. When the distance d of the source from the core was more than 500 nm, the collection efficiency was found negligible. An exponential relation between the d and collection efficiency can be observed in the Figure 3(b). When the d is decreased bellow the 200 nm, the coupling efficiency is increased rapidly. The dependence of the coupling efficiency on the width of the waveguide was also investigated.

The fluorescence collection efficiency of the straight waveguide estimated for different widths (W) of the waveguide shows that the increment of W slightly increases the efficiency. Similar effect was already observed in the fiber in the Ref. [28], and they have reported that the collection efficiency of the fiber is increasing with the V-number of the waveguide. In the present simulation, the refractive indices of the core and cladding are kept constant and the width W of waveguide is increased. Since the V-number is proportional to the width of the core and the number of guided modes supported by the waveguide, the field at the core-cladding interface is stronger and the collection efficiency increases with the V-number.

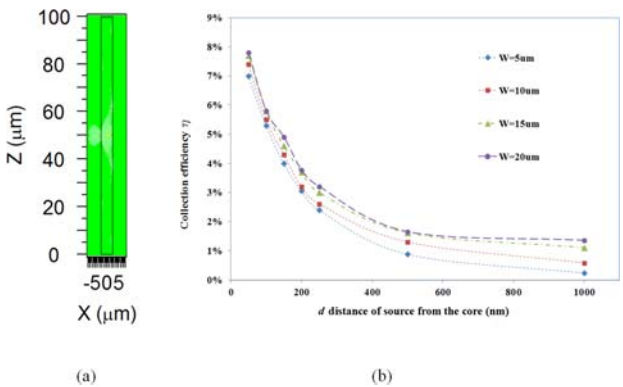

Figure 3 (online color at: www.biophotonics-journal.org) (**a**) FDTD Simulation, (**b**) fluorescence collection efficiency against the distance d of the source from the waveguide for different waveguide widths.

3.2 The fluorescence collection efficiency of s-bend

The suitability of the *s*-bend for the realization of the cascaded waveguide coupler is tested by estimating its fluorescence collection efficiency. Herein, the effect of radius of the *s*-bend is investigated on the fluorescence collection efficiency. The width and length of the *s*-bend were kept at 20 μm and 100 μm respectively in the FDTD simulation.

For the estimation of the fluorescence collection efficiency of the *s*-bend, a point source was placed at 100 nm away from the *s*-bends and a power monitor was placed at the end of the *s*-bend. The FDTD simulation showing the coupling of light from the point source located in the cladding of *s*-bend is shown in Figure 4(a). Figure 4(b) shows the variation of the fluorescence collection efficiency against the radius of the *s*-bend. The efficiency dropped considerably when the bend radius was reduced below 1000 nm.

The simulation of straight and *s*-bend confirmed that when the radius of the *s*-bend is greater than 4 to 5 mm, the florescence collection efficiency was not significantly reduced from that of a straight waveguide. The advantage of the *s*-bend for the evanescent wave sensor is that a multiple waveguide system can be realized by cascading *Y*-couplers made up of *s*-bends.

The sensor with multiple waveguides of 5 stages, namely S1, S2, S3, S4 and S5 as shown in Figure 5 is designed for evanescence coupling based sensing. The 1×2 Y splitters were designed with *s*-bends. As shown in Figure 5, the light is coupled to a single waveguide which is split into multiple paths by 1×2 *Y* splitters and after five stages of splitting, the waveguides are combined by 2×1 power combiners. A taper section of the waveguide is placed between

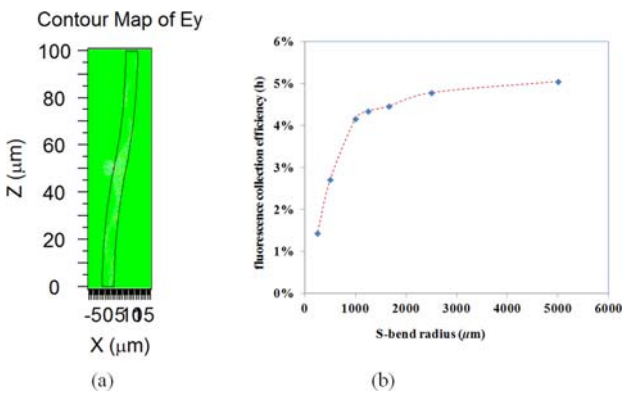

Figure 4 (online color at: www.biophotonics-journal.org) (**a**) FDTD simulation of fluorescence coupling of light by *s*-bend and (**b**) The estimated fluorescence collection efficiency against the radius of the *S*-bend.

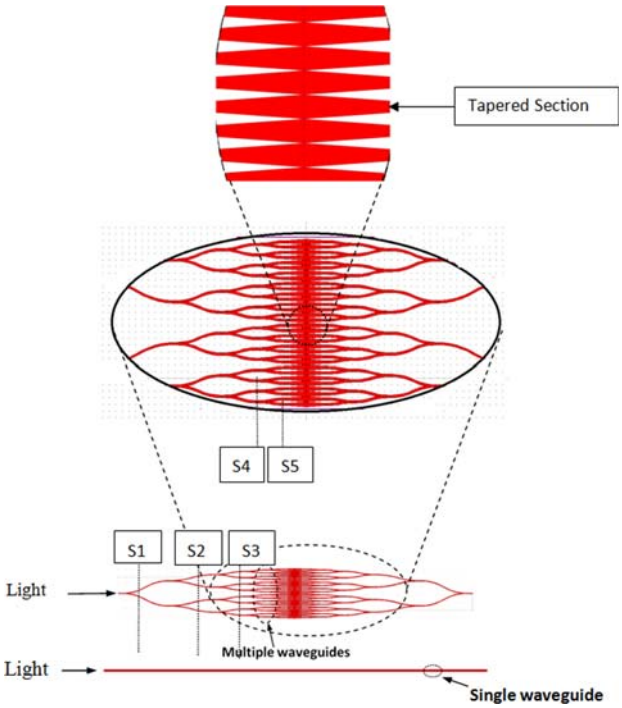

Figure 5 (online color at: www.biophotonics-journal.org) Schematic of evanescent wave sensor using cascaded waveguide coupler in comparison with a straight waveguide.

the splitters and combiners as shown in Figure 5 in order to enhance the evanescence coupling. The Y splitter was simulated by RSoft BeamPro^{TM} and the bend radius was chosen to keep the bend loses at minimum. The bend radius of first stage, where a single waveguide is split into two branches, was 23 mm. The bend radii of successive stages are 35, 40, 45 and 50 mm. The width of waveguide is 20 μm for cascaded waveguide coupler. In the tapered section, the width is increased to 40 μm at the taper-end where a splitter and a combiner connect. An enlarged view of the cascaded waveguide and tapers are also illustrated in Figure 5 for clearly showing the design. In the sensor chip, a single waveguide is also included as a reference to compare the sensitivity enhancement due to the cascaded waveguide coupler.

4. Fabrication of sensor chip

The SOS-waveguide chip is microfabricated in a clean room. The process steps involved in the fabrication of SOS-waveguide is illustrated in the Figure 6. The fabrication process starts with deposition of silicon dioxide on a silicon wafer of 4 inch diameter and (100) orientation, by plasma-enhanced chemical vapor deposition (PECVD). PlasmaLab 80 Plus of Oxford instruments is used for the PECVD of

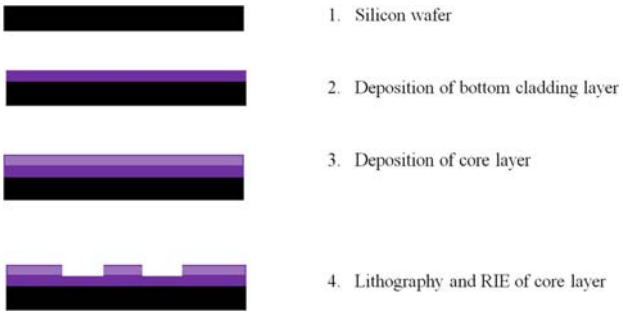

Figure 6 (online color at: www.biophotonics-journal.org) Fabrication process steps of SOS waveguide.

silicon dioxide. For the deposition of cladding layer, the deposition chamber was pumped down to 1000 mT and temperature of substrate was raised to 300 °C. The deposition gas mixture of silane and nitrogen (5 percent SiH_4, 95 percent N_2) at a flow rate of 170 sccm and nitrous oxide (N_2O) at the flow rate of 710 sccm were introduced to the PECVD chamber. Subsequently, the plasma was created by RF power of 20W at 13.56 MHz. The rate of deposition was 50 nm/minute. The deposition was carried out for 4 hours and 30 minutes to yield an oxide layer of thickness of ~14 μm for the bottom cladding of the waveguide. The process parameter is changed to achieve higher refractive index for the core layer. The flow rate of the mixture of silane and nitrogen (5 percent SiH_4, 95 percent N_2) is increased to 500 sccm and flow rate of N_2O was increased to 500 sccm, and the RF power is increased to 200 W at 13.56 MHz. The deposition is carried out for 45 minutes in order to get a thickness of 6 μm for the core layer. The refractive index characterization of silicon dioxide was carried out by ellipsometry (Spectroscopic ellipsometer, Model: VASE, Sopra). The refractive index measured for the core and cladding layer at different wavelengths is presented in the Figure 7. The refractive indices were 1.445 and 1.457 for the cladding and the core respectively at a wavelength of 635 nm.

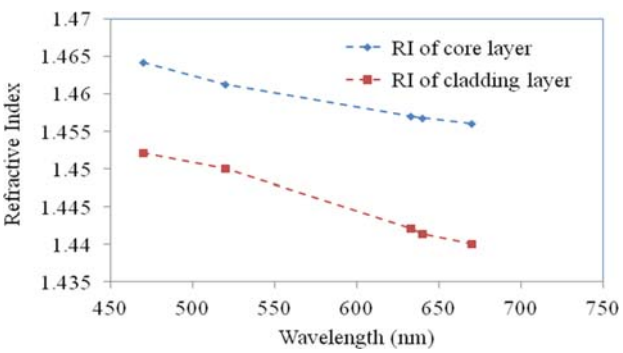

Figure 7 (online color at: www.biophotonics-journal.org) Refractive index of the core and cladding layer against the wavelength.

In the sensing experiments, as the buffer solution containing the tagged antigen is placed on the core, the buffer solution acts as the top cladding of the waveguide. For the lateral guiding of light in the waveguide, the SOS waveguide needed to be structured to desired width. The structuring of the core was carried out by direct write lithography (DWL-66) and reactive ion etching (RIE). The pattern of the cascaded waveguide couplers was designed in L-edit and transformed to the DWL66 laser writer and directly written on the wafer. The laser write-head of 2 mm having a resolution of 500 nm was used for writing the pattern. The photoresist AZ1518 was spun on the wafer at 3000 rpm and baked at 110 °C for 2 h in an oven, which resulted in a 2 μm thick photoresist layer. The pattern was etched using reactive ion etching (RIE) in MERIE P5000 plasma machine of Applied materials. Etching was carried out with alternating steps of 5 minutes of etch and 5 minutes of pause. The pause step will turn off the plasma and cool the wafer to room temperature. 12 etch and pause steps were carried out to etch 10 μm of oxide without burning the photo resist mask. For the RIE, the chamber was pumped down to 50 mT and the process gases, CHF_3, Ar and CF_4 are introduced to the chamber at the flow rate of 45, 70 and 7 sccm respectively. The plasma was created by the RF power of 300 W. This process gives an etch rate of 0.3 μm/minute. The total etching time was one hour including the 30 minutes of etch pause, which resulted in the etch depth of the 10 μm. SEM micrograph of the waveguide is shown in Figure 8.

5. Experimental setup

The experimental setup used for the SOS evanescent wave sensor is shown in Figure 9. Light from a laser source is coupled to the sensor chip and the other side of the waveguide is coupled to a spectrometer as shown in the schematic of the setup in Figure 9(a). A photograph of the experimental setup shown in Figure 9(b) shows different components used in the setup. This setup is built to couple effectively the light from the fiber to the SOS waveguide and to couple the fluorescence signal from the waveguide to spectrometer. Three high precision micropositioners with actuators of 1 μm accuracy are used in the setup. Two 5-axis controllable micropositioners obtained from Newport™ are used to couple the light from the fiber to waveguide and to couple the fluorescence light from waveguide to the collection fiber. The sample was fixed to a *XY*-axis controllable micropositioner purchased from ThorLabs. A fiber laser (OZ Optics) of 635 nm wavelength was used as the excitation source and a commercially available spectrometer (USB 2000, Ocean Optics) is used for the fluorescence spectroscopy.

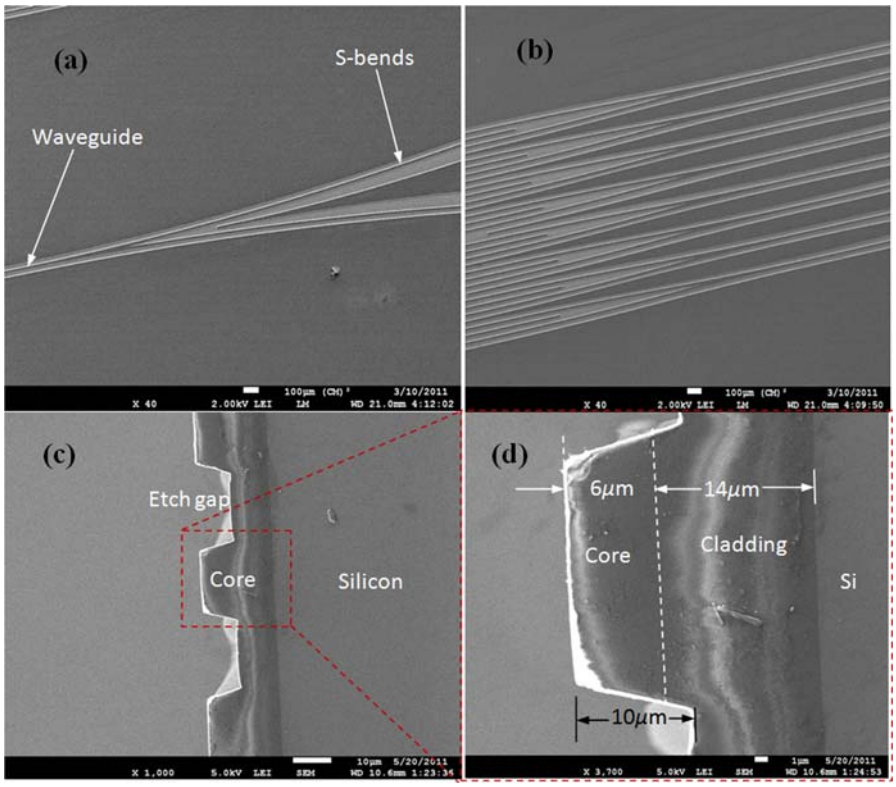

Figure 8 (online color at: www.biophotonics-journal.org) SEM micrograph of SOS waveguide, (**a**) *s*-bend coupler of the multiple waveguide system stage S1 (**b**) multiple waveguides in the stage 3 (S3) of cascaded waveguide coupler (**c**) etch profile of the waveguide (**d**) dimensions of the core of the waveguide.

In order to confirm that the confinement of the light is taking place inside the core of the waveguide, the waveguide was cut at the middle and the facet was imaged by using the optical setup shown in Figure 10. A schematic diagram of the setup used for imaging the waveguide facet is shown in Figure 10(a). Light from the laser is coupled to the waveguide and to a CCD camera placed on the other side of the waveguide in order to image the facet of the waveguide. A photograph of the experimental is shown in

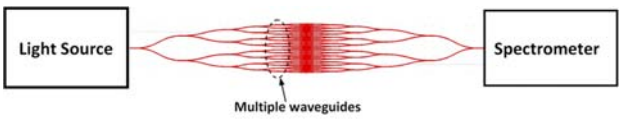

(a)

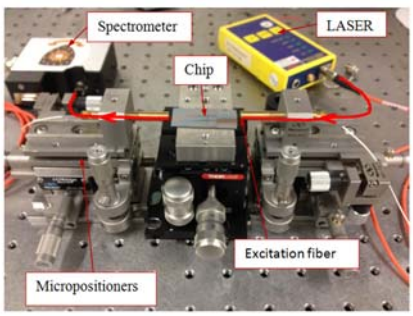

(b)

Figure 9 (online color at: www.biophotonics-journal.org) Experimental setup for the cascaded waveguide coupler sensor, (**a**) schematic of the experimental setup, and (**b**) photograph of the experimental setup.

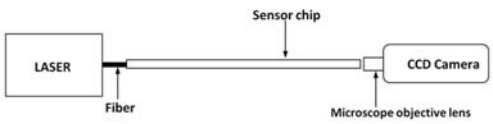

(a)

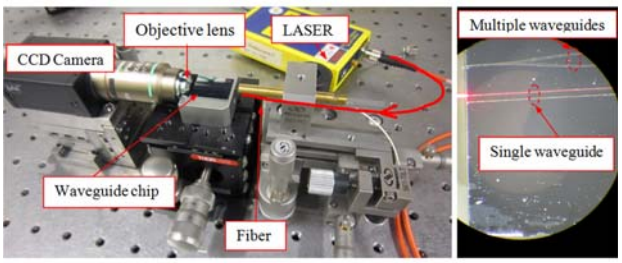

(b) (c)

Figure 10 (online color at: www.biophotonics-journal.org) Experimental setup for imaging the end facet of waveguide, (**a**) schematic diagram of the setup, (**b**) photograph of the experimental setup and (**c**) microscope image showing the coupling of light to the waveguide taken from the top of the waveguide.

Figure 11 (online color at: www.biophotonics-journal.org) (**a**) Microscope image showing the waveguide with light coupled (**a**) multiple waveguide (**b**) single waveguide.

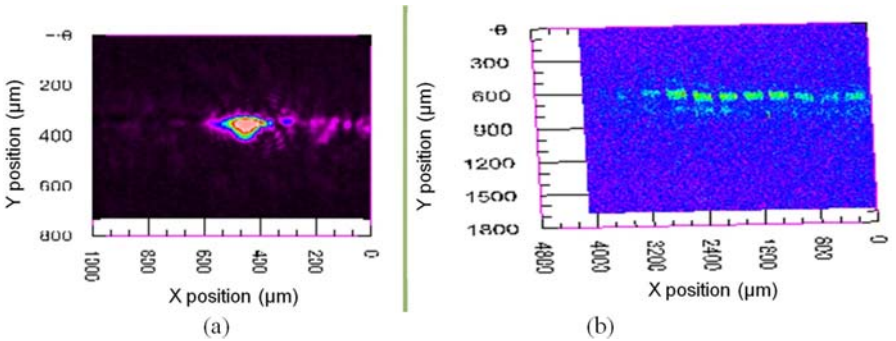

Figure 12 (online color at: www.biophotonics-journal.org) Image of the waveguide facet (**a**) Single waveguide (**b**) Multiple waveguide.

Figure 10(b). The Sample was fixed in a micropositioner stage as shown in Figure 10(b). Light from a fiber laser (OZ optics, Power-1 mW) of 635 nm wavelength was directly coupled to the waveguide by a single mode fiber (9–125 μm, core-cladding diameter) with the help of a 5 axis micropositioner stage (Newport™). A CCD camera with a microscope objective lens (Nikon 20X) was used on the other side of the waveguide to image the confinement of light in the core. Figure 10(c) shows the image taken from microscope used to observe the waveguide-fiber alignment, which shows the coupling of light from fiber to the single waveguide.

The microscope images taken from the top of the waveguide for single and multiple waveguide are shown in Figure 11. Since the light from the fiber is directly coupled to the waveguide and the divergence of the light beam coming out of singe mode fiber is large, lot of light is scattered to the cladding. The confinement of light in both single and multiple waveguides imaged by CCD camera and processed in LabVIEW is shown in Figure 12.

6. Biosensing experiments

6.1 Materials

Recombinant bovine somatotropin (rbST, Molecular Weight-22 kDa) and the anti-rbST were purchased from Cedarlane, ON, Canada. Alexa-647, Phosphate Buffered Saline (PBS) and sodium carbonate-bicarbonate were obtained from Sigma-Aldrich, Canada. The PBS tablet was dissolved in deionized (DI) water at 0.1 M concentration with a pH of 7.2. The sodium carbonate bicarbonate was dissolved in DI water for the preparation of buffer solution at a concentration of 0.1 M and pH of 9.0. The rbST obtained in the powder form was dissolved in sodium carbonate bicarbonate buffer at a concentration of 1 mg/ml. A gel filtration column filled with Sephadex G 25 beads was used to separate the unreacted FITC.

6.2 Tagging of rbST with Alexa-647

The rbST solution was prepared at 1 mg/ml in 0.1 M sodium carbonate bicarbonate buffer solution. Then 50 μL of Alexa-647 solution of 5 mg/ml was added to 1 ml of rbST solution. The reaction of rbST and Alexa-647 was carried out under continuous stirring at various times and temperatures for obtaining the best labeling ratio. After the reaction, the labeled rbST was separated from the reaction mixture by column chromatography using Sephadex G 25. Elution of column was carried out in 10 fractions of 2 ml PBS. The UV-Visible absorbance spectrum of each fraction was measured by spectrophotometer (LAMBDA 650, Perkin Elmer) to assess the presence of conjugates. The degree of labeling and the concentration of rbST in the conjugates were calculated as explained in Ref. [29, 30]. The degree of la-

beling and the concentration of rbST in the conjugate were estimated at 1 and 19 μg/ml, respectively. The conjugate was diluted to different concentration in PBS for the sensing experiments.

6.3 Immobilization of fluorescently tagged-rbST on the sensor chip

A schematic representation showing various steps involved in the adsorption of fluorescently tagged-rbST onto the SOS waveguide is shown in Figure 13. The first step of sensing is the immobilization of anti-rbST. The anti-rbST was prepared at a concentration of 100 ng/ml in phosphate buffered saline (PBS). First, the sensor chip was cleaned in DI water with ultrasonic cleaner for 5 minutes then subsequently in acetone and ethanol. Then the samples were heated at 100 °C in an oven for at least one hour. The surface of the waveguide core was modified with 3-Aminopropyltriethoxysilane (APTES, sigma Aldrich) [31] in order to attach the anti-rbST covalently. The waveguides were immersed in ethanol containing 2% APTES for 15 minutes, rinsed in ethanol and heated at 100 °C for 15 minutes. Figure 13(a) shows the waveguide with the OH groups activated on the surface after cleaning and silanization. Then the waveguide was soaked in anti-rbST solution for 1 h and washed in PBS. The Figure 13(b) represents the sample after the anti-rbST was adsorbed. In order to block the non-specific binding site, the sample was soaked in bovine serum albumin (BSA) and the sample was washed with PBS. Figure 13(c) shows the samples after blocking the non-specific binding sites. Then the waveguide was fixed in the measurement setup shown in Figure 9 and the tagged-rbST solution was added directly on the waveguide covering all the waveguide regions. The representation of sample with tagged-rbST is as shown in Figure 13(d).

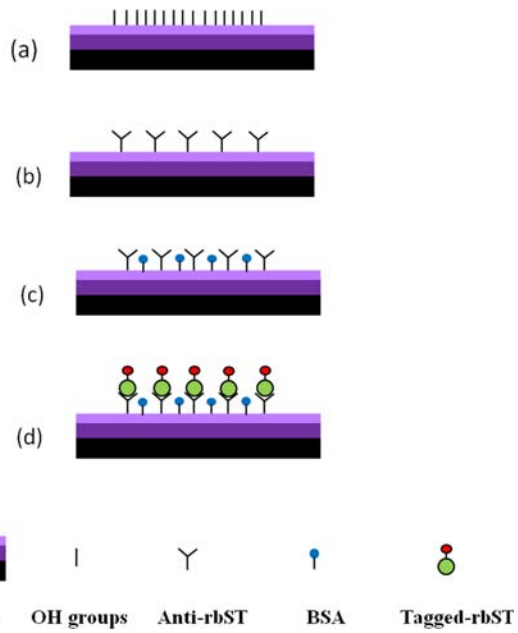

Figure 13 (online color at: www.biophotonics-journal.org) Steps involved in the functionalization of waveguide chip, (**a**) modify the waveguide surface with APTES silane to adsorb the anti-rbST (**b**) adsorb anti-rbST and (**c**) block non-specific sites and (**d**) adsorb the tagged rbST.

7. Results and discussion

In order to investigate the suitability of the sensor for quantitative measurements of tagged rbST, the variation of fluorescence signal against the concentration of tagged-rbST was established. Several identical SOS-waveguides chips were used for the detection experiments in order to study the variation of fluorescence signal against the concentration of tagged-rbST. The evanescent-coupled fluorescence signal is collected through the waveguides and coupled to the spectrometer. The intensity of the fluorescence spectrum was found fluctuating immediately after adding the tagged-rbST on the waveguide and fluorescence spectrum was stabilized after 10–15 minutes. The fluorescence spectrum was recorded after 15 minutes of adding the tagged-rbST. In order to assess the enhancement of the sensitivity of cascaded waveguide coupler, the detection was also carried out by using a single waveguide.

The fluorescence signals recorded for various concentration of tagged-rbST in single and cascaded waveguide coupler are shown in Figure 14(a) and (b), respectively. For the single waveguide, limit of detection is found as low as 140 ng/ml. When the concentration of tagged-rbST was above 1200 ng/ml, the sensor response was found saturating faster as shown in Figure 15. The detection limit of the cascaded waveguide coupler systems was found to be 25 ng/ml. The detection limit of the cascaded waveguide coupler was found enhanced to be more than 5 times as compared to that of the single waveguide. The sensor response was observed to be saturated when the concentration of the tagged rbST was above 600 ng/ml for the cascaded waveguide coupler. The fluorescence signal intensity of the sensor measured for various concentration of tagged-rbST for single waveguide and cascaded waveguide coupler is presented in Figure 15.

When the fluorophore tagged-rbST is added to the waveguide immobilized with the ant-rbST, the tagged rbST was adsorbed onto surface of the waveguide and gets excited with the evanescence light. The fluorescence signals emitted by the tagged-rbST

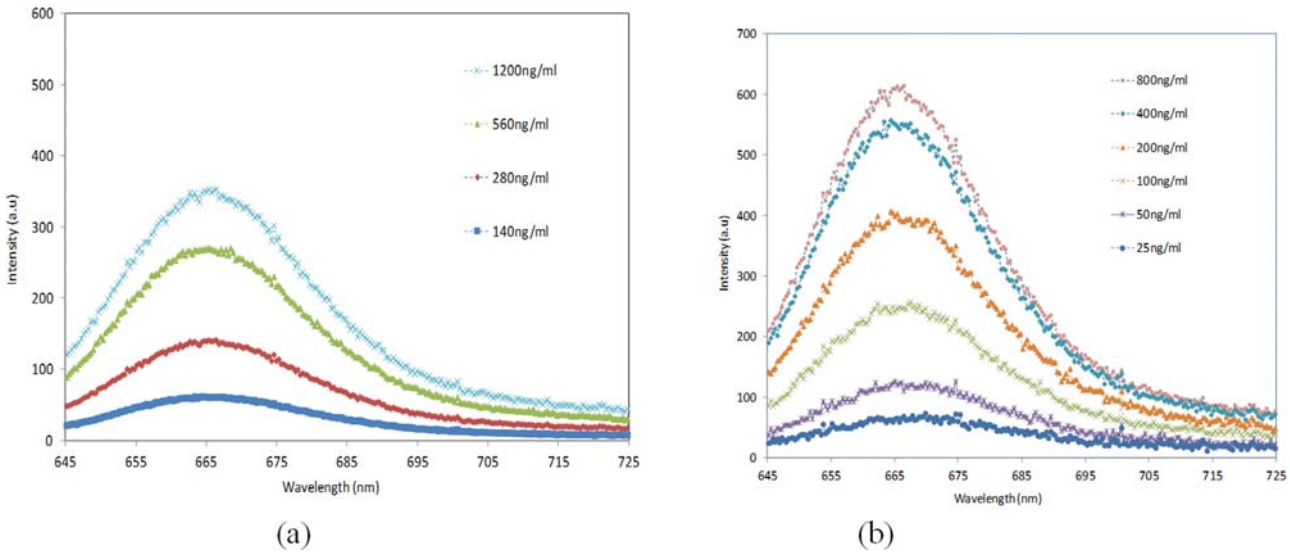

Figure 14 (online color at: www.biophotonics-journal.org) Fluorescence signal recorded in the sensor chip after antigen-antibody binding for various concentrations of tagged-rbST, for (**a**) single waveguide (**b**) cascaded waveguide coupler.

are collected back to waveguide. When the concentration of the tagged-rbST was increased, all the binding sites on the surfaces are eventually filled and hence the sensor output is getting saturated. Therefore, when the concentration of tagged-rbST was increased above 600 ng/ml, both the single and cascaded waveguide are getting saturated as shown in Figure 15. Due to the higher light collection efficiency of the cascaded waveguide coupler, the output of the CWC is found to be saturating faster at low concentration of the tagged rbST (at around 600 ng/ml) compared to the single waveguide (at around 1200 ng/ml).

It is reported that the concentration of the bST in milk may be of the order of 1–10 ng/ml [32]. The rbST may be found in the milk of the rbST treated animal for the enhancement of milk and meat production and the concentration of rbST in milk may be of the order of hundreds of ng/ml depending upon the extent of use rbST in animal. As the detection limit of the proposed CWC evanescent wave sensor is as low as 25 ng/ml, this method is suitable for the detection of rbST in milk.

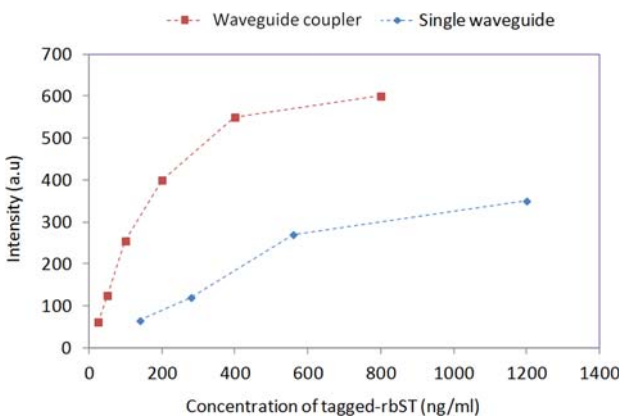

Figure 15 (online color at: www.biophotonics-journal.org) Variation of fluorescence signal against the concentration of tagged-rbST.

8. Conclusion

A novel evanescent-wave based fluorescence sensor using a cascaded waveguide coupler is designed and implemented on the silica-on-silicon platform. Advantages of SOS platform for the monolithic-integration of a cascaded waveguide coupler using Y splitters designed by s-bends and tapers are used for the realization of the sensor. The fluorescence collection efficiency of straight and bend waveguide was analyzed by using FDTD simulation. The suitability of the sensor is demonstrated for the detection of Alexa-647 tagged recombinant bovine somatotropin. For the specific detection of rbST, the anti-rbST was adsorbed to the waveguide and the tagged-rbST was detected by the enhanced evanescence fluorescence coupling. The sensitivity of the proposed waveguide coupler system realized by cascading waveguides was found more than 5 times to that of the single waveguide.

Acknowledgements Authors would like to thank Ministère du Développement économique, innovation et exportation (MDEIE) Québec and Valeo Gestion, Montreal Canada for the financial support for the project.

Jayan Ozhikandathil received the AMIE (I) degree in Electronics and communication engineering from Institution of Engineers (India), Kolkata, India and M.Tech degree in Opto-electronics and laser technology from International school of photonics Cochin University of science and technology, Cochin, India. He is currently working towards the Ph.D. degree at Optical Bio-Microsystems laboratory, Mechanical and Industrial Engineering, Concordia University, Montreal, Canada. His research interest includes Optical BioMEMS and integration of nanomaterial in the microfluidics devices.

Muthukumaran Packirisamy is a Professor and Concordia Research Chair on Optical BioMEMS in the Department of Mechanical and Industrial Engineering, Concordia University, Canada. He obtained his Ph.D. from Concordia University, MS from Indian Institute of Technology Madras, India and BS from University of Madras, India. He also worked for many MEMS industries in Canada. He is presently involved with developing BioMEMS devices in collaboration with industries. His research interest includes Optical BioMEMS, Integration of Microsystems and Micro-Nano integration.

References

[1] G. S. Asimov and N. K. Krouze, J. Dairy Sci. **20**, 289–306 (1937).
[2] F. H. Buttel, Agriculture and Human Values **17**, 5–20 (2000).
[3] J. Burkhardt, Technology in Society **14**, 221–243 (1992).
[4] J. J. Molnar, K. A. Cummins, and P. F. Nowak, J. Dairy Sci. **73**, 3084–3093 (1990).
[5] X. Zhao, B. McBride, L. Trouten-Radford, L. Golfman, and J. Burton, Domest. Anim. Endocrinol. **11**, 209–216 (1994).
[6] L. Castigliego, G. Iannone, G. Grifoni, R. Rosati, D. Gianfaldoni, and A. Guidi, J. Dairy Res. **74**, 79–85 (2007).
[7] S. K. Jindal and R. S. Ludri, Asian-Australian J. Anim. Sci. **3**, 319–322 (1990).
[8] P. Groenewegen, B. McBride, J. Burton, and T. Elsasser, J. Nutr. **120**, 514–520 (1990).
[9] C. M. Zwickl, H. W. Smith, and P. H. Bick, J. Agric. Food Chem. **38**, 1358–1362 (1990).
[10] M. L. Scippo, G. Degand, A. Duyckaerts, and G. Maghuin-Rogister, Annales De Medecine Veterinaire, Belgium (1997).
[11] N. Rochut, B. Le Bizec, F. Monteau, and F. André, Analusis **28**, 280–284 (2000).
[12] M. H. Le Breton, S. Rochereau-Roulet, G. Pinel, F. Monteau, and B. Le Bizec, Agilent technologies application note (2008).
[13] T. H. J. Heutmekers, M. G. E. G. Bremer, W. Haasnoot, and M. W. F. Nielen, Anal. Chem. Acta **586**, 239–245 (2007).
[14] A. Chandrasekaran and M. Packirisamy, Biomed. Microdevices **12**, 923–933 (2010).
[15] D. A. Stuart, A. J. Haes, C. R. Yonzon, E. M. Hicks, and R. P. Van Duyne, IEE Proc. Nanobiotechnol. **152**, 13–32 (2005).
[16] A. Chandrasekaran and M. Packirisamy, J. Biomed. Opt. **14**, 054050 (2009).
[17] A. Messica, A. Greenstein, and A. Katzir, Appl. Opt. **35**, 2274–2284 (1996).
[18] H. Helmers, P. Greco, R. Rustad, R. Kherrat, G. Bouvier, and P. Benech, Appl. Opt. **35**, 676–680 (1996).
[19] A. P. Abel, M. G. Weller, G. L. Duveneck, M. Ehrat, and H. M. Widmer, Anal. Chem. **68**, 2905–2912 (1996).
[20] P. Radhakrishnan, V. Nampoori, and C. Vallabhan, Opt. Engin. **32**, 692–694 (1993).
[21] R. Srivastava, C. Bao, and C. Gomez-Reino, Sens. Actuators A Phys. **51**, 165–171 (1996).
[22] C. Singh, H. Isobe, T. Fujinami, and M. Ogita, Jap. J. Appl. Phys. **43**, 3429 (2004).
[23] J. P. Golden, G. P. Anderson, S. Rabbany, and F. Ligler, IEEE Trans. Biomed. Engin. **41**, 585–591 (1994).
[24] B. Gupta, H. Dodeja, and A. Tomar, Opt. Quant. Electron. **28**, 1629–1639 (1996).
[25] A. Prabhakar and S. Mukherji, Lab Chip **10**, 748–754 (2010).
[26] J. Ozhikandathil and M. Packirisamy, J. Biomed. Opt. **17**, 017006 (2012).
[27] C. Carniglia, L. Mandel, and K. Drexhage, JOSA **62**, 479–486 (1972).
[28] D. Marcuse, J. Light Wave Technol. **6**, 1273–1279 (1988).
[29] R. M. Mckinney, J. T. Spillane, and G. W. Pearce, J. Immunol. **93**, 232, (1964).
[30] B. Wood, S. Thompson, and G. Goldstein, J. Immunol. (Baltimore, Md.: 1950) **95**, 225 (1965).
[31] K. E. Sapsford and F. S. Ligler, Biosens. Bioelectron. **19**, 1045–1055 (2004).
[32] M. F. McGrath, G. Bogosian, A. C. Fabellar, R. L. Staub, J. L. Vicini, and L. A. Widger, J. Agric. Food Chem. **56**, 7044–7048 (2008).